Discover Chemical Engineering

RESEARCH Open Access

Efficient solar-driven degradation of diclofenac in aquatic environments using Cu-TiO_2/Kaolin thin films: insights from different water matrices

Saad Slimani Tlemcani[1], Ricardo J. C. Fernandes[2,3], Ana Rita Silva[3], Pier Parpot[3,5], M. Canle[1] and Luciana Pereira[3,4*]

*Correspondence:
Luciana Pereira
lucianapereira@ceb.uminho.pt
[1]React! Group, Department of Chemistry, Sciences & CICA, Universidade da Coruña, A Coruña E-15071, Spain
[2]Physics Centre of Minho and Porto Universities (CF-UM-UP), Braga, Portugal
[3]CEB– Centre of Biological Engineering, University of Minho, Campus de Gualtar, Braga 4710-057, Portugal
[4]LABBELS– Associate Laboratory, Braga 4710-057, Portugal
[5]Centre of Chemistry, Chemistry Department, CQUM, University of Minho, Campus de Gualtar, Braga 4710-057, Portugal

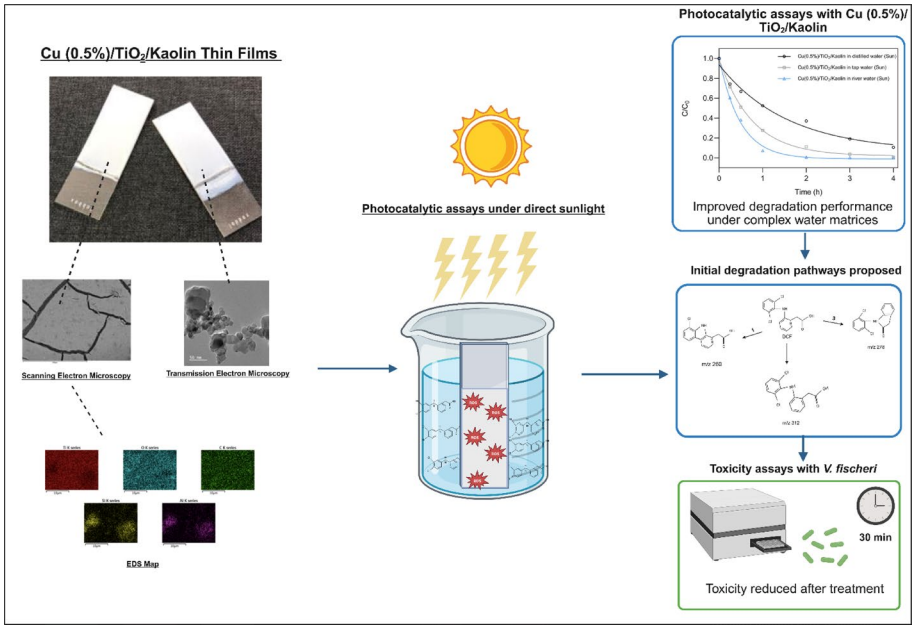
Abstract

Photocatalysis has gained considerable attention for the degradation of hazardous pollutants. In this study, the photocatalytic efficiency of Cu(0.50%)/TiO_2/Kaolin thin films was evaluated for the removal of diclofenac (DCF), a widely used non-steroidal anti-inflammatory drug, from aquatic environments. The photocatalytic activity of the thin films was assessed in three different water matrices: distilled water (DW), tap water (TW), and river water (RW), using pollutant concentrations reflective of environmental levels. The catalyst's effect was more pronounced in RW. Under solar irradiation, the films achieved high DCF removal rates, demonstrating their low energy requirements. The degradation rate constants were 0.496 h^{-1}, 1.097 h^{-1}, and 2.560 h^{-1} for DW, TW, and RW, respectively, at an initial DCF concentration of 25 mg/L. These findings indicate that Cu(0.50%)/TiO_2/Kaolin thin films exhibit robust photocatalytic activity under direct sunlight across different water matrices without significant activity suppression. Degradation mechanisms were proposed based on the transformation products identified. Additionally, toxicity assays employing *Vibrio fischeri* revealed that while DCF increases toxicity in aquatic systems, photocatalysis with Cu(0.5%)/TiO_2/Kaolin under solar irradiation significantly reduced it, though the final solutions remained "toxic". In contrast, photocatalysis under UV irradiation, despite achieving faster DCF degradation, did not reduce toxicity, which remained close to 100%. This work provides evidence of advanced DCF degradation under direct sunlight, highlighting the potential of Cu(0.50%)/TiO_2/Kaolin thin films for sustainable water treatment applications.

Keywords Cu/TiO_2/Kaolin thin films, Diclofenac, Photocatalysis, Solar irradiation, Toxicity, Water matrices

© The Author(s) 2025. **Open Access** This article is licensed under a Creative Commons Attribution-NonCommercial-NoDerivatives 4.0 International License, which permits any non-commercial use, sharing, distribution and reproduction in any medium or format, as long as you give appropriate credit to the original author(s) and the source, provide a link to the Creative Commons licence, and indicate if you modified the licensed material. You do not have permission under this licence to share adapted material derived from this article or parts of it. The images or other third party material in this article are included in the article's Creative Commons licence, unless indicated otherwise in a credit line to the material. If material is not included in the article's Creative Commons licence and your intended use is not permitted by statutory regulation or exceeds the permitted use, you will need to obtain permission directly from the copyright holder. To view a copy of this licence, visit http://creativecommons.org/licenses/by-nc-nd/4.0/.

Graphical abstract



1 Introduction

Pharmaceutical contamination of water bodies has emerged a pressing environmental issue, primarily driven by pharmaceuticals extensive use and their persistence in aquatic systems [1, 2]. Indeed, in recent decades, advancements in medical and pharmaceutical sciences have significantly increased the production and consumption of pharmaceuticals, resulting in higher concentrations of these compounds and their metabolites in wastewater. The limited removal efficiency of conventional wastewater treatment plants (WWTPs) allows these substances to persist in treated effluents, amplifying their environmental impact [1–3]. Among these contaminants, Diclofenac (DCF), a non-steroidal anti-inflammatory drug (NSAID), is one of the most frequently detected in surface waters, groundwater, and wastewater effluents, as well as adsorbed in the sewage sludge during conventional treatments [3–5]. DCF concentrations ranging from 0.14 to 1.48 mg L^{-1} have been detected in WWTP effluents and surface waters [6]. A range of 70.5-267.1 ng g^{-1} was detected in the sewage sludge of two WWTP at the Northern Portugal [3]. Even at low concentrations, DCF poses significant ecological and human risks due to its toxicity and potential for bioaccumulation [7, 8]. The primary ecological concerns associated with DCF exposure and bioaccumulation in aquatic ecosystems involve mutagenic and genotoxic effects, which compromise the reproductive systems, causing severe imbalances in the ecosystems [9]. For example, lipid peroxidation damage has been observed in the liver of inanga fish (*Galaxias maculatus*). Additionally, studies on two different species of amphibians from Argentina (*Trachycephalus typhonius* and *Physalaemus albonotatus*) have demonstrated the adverse effects of DCF exposure on larval development, including reduced growth rates and impaired locomotion in water, which affected swimming abilities [9]. In humans, exposure to DCF has been linked to severe liver damage, reproductive disorders, tissue accumulation and cell growth limitations [9, 10].

Advanced oxidation processes (AOPs) have proven effective methods in removing persistent organic pollutants. Among these, photocatalysis using titanium dioxide (TiO_2) as a heterogeneous catalyst has garnered substantial attention. TiO_2 is a widely studied photocatalyst thanks to its strong oxidative power, chemical stability, non-toxicity, and cost-effectiveness [11, 12]. Upon ultraviolet (UV) light irradiation, TiO_2 generates electron-hole pairs that react with water and oxygen molecules to produce reactive oxygen species (ROS), such as hydroxyl radicals and superoxide anions capable of breaking down complex organic molecules like DCF into less harmful intermediates, ultimately mineralizing them into CO_2 and H_2O [13]. However, the photocatalytic activity of TiO_2 is mainly restricted to high-energy wavelengths due to its wide bandgap of 3.2 eV, requiring higher energy inputs [14]. To enhance TiO_2 photocatalytic efficiency under solar irradiation, structural or compositional modifications are required to extend its optical absorption range beyond the UV region, thereby enabling more effective harnessing of the solar spectrum. Metal doping can enhance the internal electron flow by capturing electrons and suppressing recombination, thereby allowing for lower energy inputs and improved photocatalytic response [15]. Also, copper (Cu) doping in TiO_2 introduces oxygen vacancies (OV), which also improves the photocatalytic activity of the material [16, 17].

Another important issue concerns the sustainability and costs of nanoparticles used as photocatalysts. To further improve photocatalytic efficiency and sustainability, it is crucial to develop better catalysts that offer advanced stability, activity under visible light, and eco-friendly characteristics. Equally important is the immobilization of nanoparticles, as it prevents their dispersion in the environment and facilitates their recovery. These advancements should be paired with innovative configurations that allow for the practical application, recovery, and reuse of the nanocatalysts, making the process more feasible and cost-effective for real-world water treatment applications. Kaolin, a naturally abundant and low-cost clay material, formed from kaolinite, has been widely explored as a nanoparticle support in thin-film preparation. A thin-film configuration offers practical advantages, including easier recovery and reuse of the photocatalyst. Kaolin, is prized for its mechanical and thermal stability, low price, and abundance, and is also considered eco-friendly [18]. Kaolin has been previously proven as an excellent support for catalysts like ferric-oxalate [19], nickel [20] Zirconium dioxide [21]. In our previous work [17], kaolin clay pellets were used to support TiO_2-P25 doped with Cu and Co via the incipient wetness impregnation method. Catalyst lixiviation was evaluated through ICP-MS, and the composites demonstrated high structural integrity and low metal leaching. Stability tests further confirmed the continuous degradation efficiency of amoxicillin over multiple photocatalytic cycles, indicating excellent reusability and sustained performance over time. Additionally, other studies studies have explored the use of kaolinite as a substrate to support nano TiO_2, showing that kaolinite/TiO_2 nanophotocatalysts can be easily separated and recovered from water treatment systems [17]19]– [25]. These composit.es also exhibit improved adsorption and photocatalytic efficiency for removing organic contaminants. With respect to kaolin, a study by Zyoud et al. [26], demonstrated the efficiency of Kaolin-supported ZnO nanoparticles in degrading the pharmaceutical compound tetracycline, with kaolin granting structural support and enabling a catalyst reuse. Similarly, the study by Mohammed et al. [27]., highlighted the excellent photocatalytic efficiency, stability, and possible strong reutilization of Kaolin-Supported Nickel

Oxide, further emphasizing the advantages of kaolin as a support material for catalyst immobilization and recovery.

In the present work, a photocatalyst composed of TiO_2 and kaolin (90% + 10%, respectively), impregnated with Cu^{2+}, was deposited as a thin film on flat glass surfaces resulting in the catalysts Cu(0.5%)/TiO_2/Kaolin. The combination of kaolin, TiO_2, and copper is intended to improve the crystallinity of the material, a critical factor for optimizing its catalytic efficiency. The photocatalytic efficiency of Cu(0.5%)/TiO_2/Kaolin thin film was evaluated for the degradation of DCF in various water matrices, i.e., in distilled water (DW), tap water (TW), and river water (RW), under solar and UV irradiation. The photocatalytic degradation by-products were identified, and toxicity assessment using *Vibrio fischeri* (ISO ISO 11348-1 and ISO 11348-3) [28, 29] was conducted before and after the catalytic process. This research sought to develop an efficient solar-driven photocatalytic for the effective degradation of DCF.

We use a dip-coating method in preparing this material, carefully adjusting the proportions of each component to create an optimal mixture. The calcination is performed at 600 °C, as each material has a specific role in preserving the desired phase composition (calcination was employed to stabilize the material on the surface of the films). Our main goal is to keep the anatase phase intact instead of allowing it to change into the rutile phase, since higher temperatures can encourage this transition and potentially lower catalytic efficiency. To address this, we add kaolin to the solution, which helps stabilize the anatase phase and prevents its conversion to rutile. This thoughtful strategy ensures that the final material achieves high catalytic performance, in line with our aim of developing an effective and stable catalyst.

2 Materials and methods

2.1 Chemicals

TiO_2-P25 (Dgussa Aeroxide P25) was acquired from Evonik (about 80% Anatase, 20% rutile with a small proportion of amorphous phase) [30]. Copper (II) sulfate pentahydrate ($CuSO_4.5H_2O$) (≥ 98%, Sigma), natural unrefined kaolin (provided by CAVISA, Ref. GF40M), and Dichlofenac sodium (≥ 99%) were acquired from Sigma Aldrich. Formic acid and acetonitrile (ACN) for High Performance Liquid Chromatography coupled to mass spectrometry (HPLC-MS) analysis were purchased from Merk and Fluka, respectively, at the highest analytic grade purity commercially available (98%). The ultra-pure water (18.2 MΩ cm at 20 °C) used to prepare the eluent for HPLC-MS was obtained from Millipore.

2.2 Preparation of the thin film

To prepare the thin films, a dispersion was created by mixing TiO_2-P25 and kaolin in a 90:10 ratio, with the addition of Cu^{2+} ions to enhance photocatalytic performance. The TiO_2-P25 acted as the main photocatalytic agent, while kaolin functioned as a binder to improve stability and adhesion to the glass support. Copper(II) sulfate pentahydrate ($CuSO_4 \cdot 5\ H_2O$) was used as the Cu^{2+} precursor, added at a concentration corresponding to approximately 0.5 wt% relative to the total precursor mass (TiO_2 + kaolin + Cu). This formulation was chosen based on preliminary optimization for dispersion stability and photocatalytic enhancement. This dispersion was then used for the dip-coating process to form thin layers on flat glass surfaces. The glass slides (75 mm × 25 mm ×

3 mm lime slide glass) underwent a thorough pre-treatment to ensure optimal adhesion and film homogeneity. First, the slides were sonicated to remove surface impurities, followed by chemical etching with 67% concentrated nitric acid for 15 min to create a more reactive surface. After etching, the slides were thoroughly rinsed with Milli-Q water and acetone to remove any residual acid or contaminants, followed by drying in a muffle oven at 100 °C to eliminate moisture. A second etching was performed using 37% concentrated hydrochloric acid for 15 min, further enhancing the surface properties. The slides were again rinsed with Milli-Q water and dried at 100 °C, an subjected to dip-coating by immersion in a homogeneous solution of 0.5% Cu, TiO_2-P25, and kaolin. The immersion speed was carefully controlled at 200 mm/min to ensure uniform coating thickness. After coating, the slides were dried in an oven at 90 °C to remove any remaining solvents and stabilize the film. The coated slides were then calcined in a furnace (Paragon model HT-22D, Thermcraft) at 600 °C for 3 h, with a heating rate of 5 °C per min. The purpose of calcination was to stabilize the thin films, ensuring proper crystallinity, photocatalytic activity, and adhesion to the glass substrate. The chosen temperature of 600 °C was critical for maintaining the anatase phase of TiO_2, which is key to photocatalytic efficiency, as higher temperatures may induce a phase transformation to rutile, reducing catalytic performance. The inclusion of kaolin in the dispersion helped to stabilize the anatase phase and prevent this transformation. The high-temperature process also ensured strong adhesion between the coating and the substrate and removed any remaining organic residues.

2.3 Characterization techniques

The surface morphology and cross-sectional structure of the catalytic thin films were obtained by scanning electron microscopy (SEM) using a JEOL JSM-6400FEG scanning electron microscope (JEOL Ltd., Japan) coupled with energy-dispersive X-ray spectroscopy (EDS) for imaging and chemical composition analysis. The morphology of TiO_2-P25 and Cu(0.5%)/TiO_2/Kaolin was analyzed via Transmission Electron Microscopy (TEM). Samples were prepared by depositing water droplets on carbon formvar-coated copper grids (200 mesh) and air-drying. TEM images were captured using a Jeol-JEM-1100 microscope (JEOL Ltd., Japan) at 80 kV. Carbon content was determined through elemental analysis using a Thermo Flash 1112 instrument. The film structures were analyzed using X-ray diffraction (XRD) on a Bruker D8 Advance diffractometer (Bruker Corporation, UNITED STATES) with a Cu source and an X'Pert PRO (PANalytical) diffractometer (Malvern Panalytical, Netherlands) featuring Ni-filtered Cu Kα radiation. Measurements were performed with a 2θ range of 20°–90°, a step size of 0.050°, and an acquisition time of 2.5 s per step. X-ray fluorescence (XRF) analysis were performed using a Bruker S4 Pioneer spectrometer (Bruker Corporation, UNITED STATES), and particle size distribution was determined via laser light scattering using a Micromeritics Saturn DigiSizer II.

2.4 Photocatalytic experiments

Photocatalytic degradation experiments applying Cu(0.5%)/TiO_2/Kaolin were conducted on clear sunny days, between 12:30 PM and 4:30 PM in Braga, Portugal. Solar radiation was continuously measured throughout each experiment using a solar power meter (Model SM206), with recorded values ranging from 1400 W/m^2 to 1800 W/m^2.

Table 1 Physicochemical characterization of tap and river water samples used in photocatalytic assays

Type of water	pH	TOC (mg/L)	COD (mg/L)	Nitrate (mg/L)
Distilled Water (DW)	7.0	0	0	0
Tap Water (TW)	6.9	4.42	1.60	0.24
River Water (RW)	6.9	8.81	2.88	2.49

These values are indicative of high radiation levels. For comparison, and to better evaluate the efficiency of the catalyst under more controlled conditions, a UV-light set-up that uses 6 Philips BLB 8 UV Tube 8 W lamps emitting radiation under 365 nm, was used for artificial irradiation. The initial assays were performed using a concentration of 25 mg/L of DCF, in three different water matrices: distilled water (DW), tap water (TW) and river water (RW). The pH of the water matrices was in neutral range (6.9-7.0). As shown in Table 1, the organic and nutrient content varied significantly among them: TW and RW presented notable levels of TOC (4.42 and 8.31 mg/L, respectively) and COD (1.60 and 2.88 mg/L, respectively) while DW showed no detectable organic load, as expected. Nitrate concentrations were also higher in RW (2.49 mg/L), indicating greater background complexity for photocatalytic testing. Before conducting the photocatalytic assays under direct sunlight, the adsorption of DCF onto the synthesized Cu(0.5%)/TiO_2/Kaolin material was first evaluated through experiments under dark conditions. The degradation of DCF by photolysis was also evaluated through tests under solar irradiation, in the absence of the material.

The subsequent photocatalytic assays under solar irradiation were conducted using four different concentrations of DCF: 0.5 mg/L and 1 mg/L, which reflect typical concentrations found in environmental waters (µg/L range), and 25 mg/L and 100 mg/L, which are commonly used in the literature to probe catalyst performance, degradation pathways, and stability under stress conditions. This concentration range was selected to allow for a more comprehensive evaluation of the catalyst's effectiveness, both at environmentally realistic levels and under higher pollutant loads. Moreover, treating more concentrated solutions may be relevant in applications where pollutants are first concentrated through adsorption-based processes and later subjected to photocatalytic degradation in smaller volumes. Under UV irradiation, only the concentration 100 mg/L was assayed. This condition was chosen to investigate deeper degradation stages and transformation product formation, facilitating more accurate analytical detection and providing insights into the potential for complete DCF mineralization under intensified treatment conditions.

2.5 Monitoring DCF degradation and identification of transformation products

The monitoring of DCF concentration during the photocatalytic process, and the identification of transformation products, were carried out using HPLC coupled to mass spectrometry (HPLC-MS) aiming at elucidating the degradation pathways of DCF. MS analyses were performed using the highest concentration of DCF (100 mg/L) to better align with the detection limits, particularly for the identification of by-products that may form at low concentrations. A Finnigan Survayor Chromatography System, coupled to LxQ Thermo Mass Detector, was used. The separation of the products was carried out on C18 column Luna® 3 µm (Phenomenex, 100 × 2 mm).The mobile phase consisted of

0.1% of Formic acid in ultrapure Water (eluent A) and Acetonitrile (eluent B), with a gradient elution program starting at 90% of A and 10% of B, linearly transitioning to 10% of A and 90% of B over 15 min, and returning to the initial percentages after 25 min. The flow rate was maintained at 0.2 mL/min. Sample injection volume was 20 µL. The HPLC was connected to a linear ion trap mass spectrometer equipped with an electrospray ionization (ESI) source, and mass spectra were acquired over a mass range of 50–500 amu. The instrument was operated both in positive ionization mode with a capillarity voltage of 43 and − 49 V, respectively. The mass spectrometry data was handled using Excalibur software (Thermo).

2.6 Toxicity assessment

Toxicity assays were conducted following the standardized method "Water Quality–Determination of the Inhibitory Effects of Water Samples on the Light Emission of *Vibrio fischeri* (Luminescent Bacteria Test)", using freshly prepared bacteria [28]. *V. fischeri* strain NRRL-B-11,177, supplied as a freeze-dried reagent (BioFix® Lumi, Macherey-Nagel, Düren, Germany), was cultivated aerobically in our laboratory under controlled conditions [28, 29, 31]. The toxicity assessment was based on changes in bacterial bioluminescence upon exposure to potentially toxic compounds. The procedure was adapted from ISO standards 11348-1 and 11348-3, as detailed in previous studies [32, 33].

The toxicity assessment included samples collected before and after 4 h of DCF photocatalytic degradation using Cu(0.5%)/TiO_2/Kaolin in the various water matrices (DW, TW, and RW), both under dark conditions and solar irradiation. Additionally, samples were taken before and after 4 h of photolysis. Controls consisted of TW and RW without DCF. Negative (2% NaCl solution) and positive (a solution of potassium dichromate ($K_2Cr_2O_7$) at a concentration of 105.8 mg/L) controls were also incorporated, using the bacterial suspension [28, 29, 31]. The pH of all samples was measured and adjusted to a range of 6 and 9 using hydrochloric acid or sodium hydroxide solutions, when required. The salinity was standardized to 2% NaCl. An oxygen concentration above 3 mg/L was ensured, and the turbidity was eliminated by centrifugation and filtration of the samples prior to analysis. Percentage of luminescence inhibition (INH%) was determined after 30 min of exposure [28, 29, 34], following the calculation methods defined by Eqs. (1) and (2):

$$INH\ (\%) = 100 - \frac{IT_t}{KF \times IT_0} \times\ 100 \tag{1}$$

With,

$$KF = \frac{IC_t}{IC_0} \tag{2}$$

where IT_t represents the luminescence intensity of the sample after 30 min of contact, IT_0 is the luminescence at the start of the assay (time 0), KF is the correction factor accounting for the natural decline in luminescence of the negative control, IC_t is the luminescence intensity of the control after a certain contact time (t), and IC_0 is the initial luminescence intensity of the negative control. Luminescence was recorded using a microplate reader (Biotek® Cytation3, Fisher Scientific, Korea) in kinetic mode, and the signal was measured in relative light units (RLU/Sec).

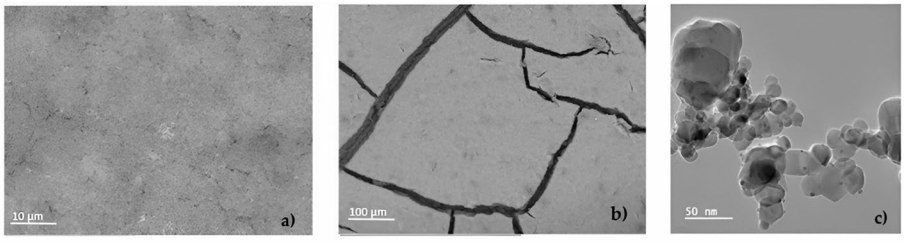


Fig. 1 SEM (**a**-**b**) and TEM (**c**) images of Cu (0.5%)/TiO_2/Kaolin

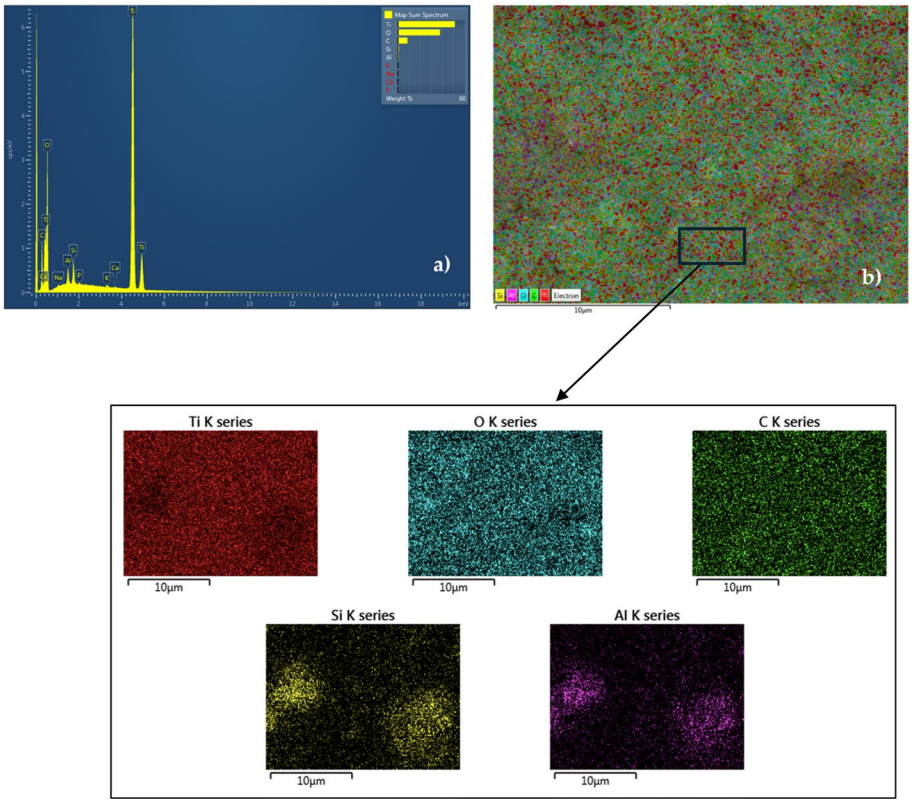


Fig. 2 EDS analysis of the material (**a**); EDS map of the material Cu (0.5%)/TiO_2/Kaolin showing the various elements present on the surface of the photocatalyst (**b**)

3 Results and discussion

3.1 Characterization of the catalysts

The morphology and elemental composition of the thin film Cu(0.5%)/TiO_2/Kaolin composite were analyzed using SEM, TEM, and EDS. SEM images (Fig. 1a–b) reveal a relatively homogeneous surface, suggesting that the components were well-integrated during synthesis. However, certain regions with noticeable spots indicate room for improvement in dispersion techniques. Additionally, despite the visible cracks resulting from calcination at 600 °C, images suggest the formation of a robust and chemically stable structure. The TEM image (Fig. 1c) offers further insights into the distribution and morphology of the Cu(0.5%)/TiO_2/Kaolin, confirming the formation of well-dispersed particles within the composite matrix. The nanoparticles display a variety of sizes, indicative of the dynamic nature of their synthesis process. The irregular shapes, which arise

from the fusion of particle edges, suggest strong interactions between adjacent particles during synthesis or calcination. This irregular morphology is likely to enhance the material's surface reactivity and structural stability, characteristics that are beneficial for its use in catalytic applications.

As shown in (Fig. 2a), the EDS spectrum of the Cu(0.5%)/TiO_2/Kaolin thin film exhibits three distinct peaks corresponding to titanium (50%), oxygen (38.7%), and carbon (9.2%). The mapping images (Fig. 2b) further demonstrate the distribution of these elements across the surface of the catalyst, highlighting the homogeneous nature of the surface composition.

The band gap energies of pristine TiO_2 and of the Cu-doped TiO_2/Kaolin composites were determined using Tauc plot analysis based on UV-Vis diffuse reflectance spectroscopy. Consistent with reported literature [35], pure anatase TiO_2 exhibits a band gap of approximately 3.2 eV. In contrast, the Cu-TiO_2/Kaolin composites demonstrated a red shift in the absorption edge, resulting in a reduced band gap ranging from 2.6 to 2.8 eV, depending on the Cu loading [36]. This band gap narrowing can be attributed to two main factors: (i) the incorporation of Cu^{2+} introduces localized 3 d states within the TiO_2 band structure, forming mid-gap states that facilitate visible light absorption [11, 37]; and (ii) the presence of kaolin enhances the dispersion of TiO_2 particles and provides a high-surface matrix, promoting more efficient light harvesting and charge separation [16]. Together, these effects extend the photoresponse of the Cu-TiO_2/Kaolin composites into the visible region, thereby improving their photocatalytic performance under solar irradiation compared to undoped TiO_2.

The crystal structure of the synthesized samples was analyzed using XRD, and the results are presented in Fig. 3. Pure TiO_2 exhibits seven prominent diffraction peaks at 25.25°, 37.52°, 48.02°, 53.58°, 54.88°, 62.61°, and 75.07°, corresponding to the anatase

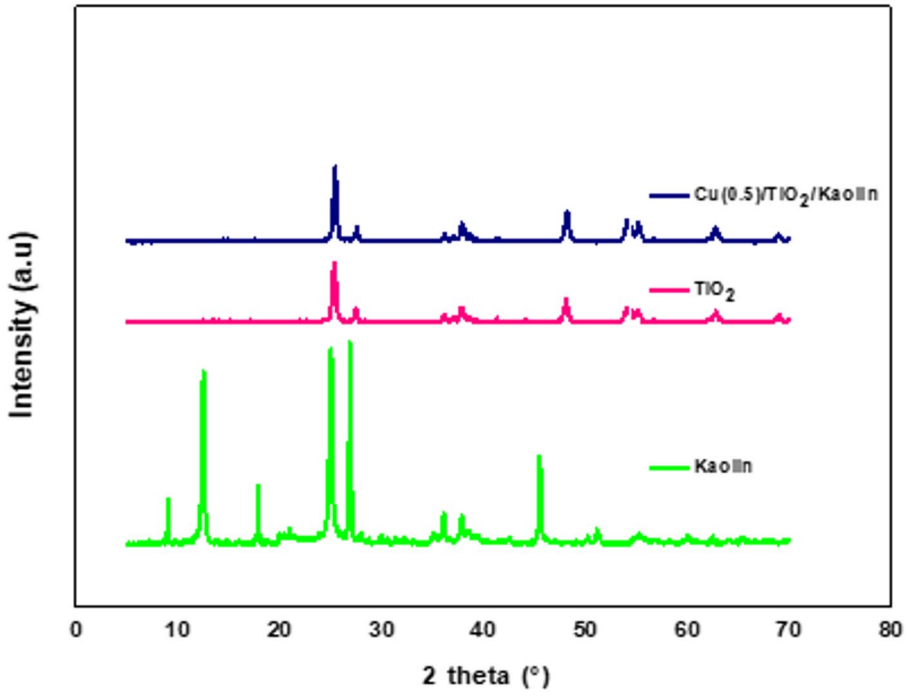


Fig. 3 X-ray diffraction patterns of TiO_2-P25, Kaolin, and the thin film containing 0.5% of transition metal (Cu (0.5%)/TiO_2/Kaolin)

phase of TiO_2, as identified by JCPDS card no. 00-021-1272 [38]. The anatase phase is predominant due to the composition of TiO_2-P25, which consists of 80% anatase and 20% rutile. This phase remains stable at low processing temperatures, whereas the rutile phase becomes dominant at higher temperatures. Specifically, the transition to rutile occurs when calcination is performed at 600 °C with a ramp rate of 5 °C/min for 3 h. Typically, rutile TiO_2 is obtained through high-temperature calcination of anatase [39].

The XRD patterns of the Kaolin, TiO_2, and Cu(0.5%)/TiO_2/Kaolin samples are similar to that of pure TiO_2, with no distinct peaks corresponding to Cu, despite the significant Cu loading within the TiO_2 matrix, despite its incorporation. This is likely due to the low Cu loading (0.5%), which is below the detection limit of XRD [40, 41]. However, a notable increase in peak intensity is observed for the Cu(0.5%)/TiO_2/Kaolin composite compared to undoped TiO_2, as illustrated in Fig. 3. This enhancement in diffraction intensity suggests improved crystallinity upon Cu doping, a phenomenon reported in previous studies [42]. The improved crystallinity may be attributed to the substitutional incorporation of Cu^{2+} ions into the TiO_2 lattice, where the slight difference in ionic radius between Cu^{2+} and Ti^{4+} could lead to localized structural ordering without significant lattice distortion. While Cu doping does not induce phase transformation or peak shifts, it does enhance the crystallinity of TiO_2 in the composite, which may positively impact the photocatalytic performance due to better charge transport properties.

Table 2 presents the chemical composition of Kaolin and Cu (0.5%)/TiO_2/Kaolin thin films as measured by X-ray fluorescence (XRF). The analysis reveals significant differences between the two samples. The dominant components in Kaolin are SiO_2 (52.4%) and Al_2O_3 (42.2%), reflecting its primary composition as a silicate material, rich in both silica and alumina. This composition is consistent with the chemical formula of Kaolin, $Al_2Si_2O_5(OH)_4$. This structure highlights the material's silicate nature, with the aluminum and silicon atoms forming the backbone of the mineral, combined with hydroxyl groups (OH) that contribute to its properties. The other oxides present in low concentrations include Fe_2O_3 (1.6%), K_2O (3.0%), TiO_2 (0.17%) and trace amounts of SO_3 (0.08%), CaO (0.05) and Cr_2O_3 (0.002%). Notably, CuO and NiO were not detected in Kaolin. In the Cu (0.5%)/TiO_2/Kaolin composite, TiO_2 is the dominant component at 92.7%, reflecting the incorporation of titanium oxide into the composite. The presence of CuO (0.142%) indicates the successful doping of copper into the structure. Other components include SiO_2 (2.7%), Al_2O_3 (2.1%), and trace amounts of Fe_2O_3 (0.23%), K_2O (0.18%), SO_3 (0.11%), Cr_2O_3 (0.067%), CaO (0.039%), and NiO (0.013%), most of them from kaolin. Additionally, CO_2 (1.7%) was detected, which may be associated with the calcination process. These results highlight the successful incorporation of Cu and TiO_2 into the Kaolin matrix, with a marked increase in the TiO_2 content in the composite, presence of CuO, and the persistence of some minor impurities from the original Kaolin.

Table 2 Chemical analysis of Kaolin and of Cu (0.5%)/TiO_2/Kaolin thin film measured by XRF

Sample	TiO_2 (%)	SiO_2 (%)	AL_2O_3 (%)	Fe_2O_3 (%)	K_2O (%)	CuO (%)	SO_3 (%)	Cr_2O_3 (%)	CaO (%)	NiO (%)	CO_2 (%)
Kaolin [43]	0.17	52.4	42.2	1.60	3.00	-	0.08	0.002	0.050	-	-
Cu(0.5%)/TiO_2/Kaolin	92.7	2.7	2.1	0.23	0.18	0.142	0.11	0.067	0.039	0.013	1.7

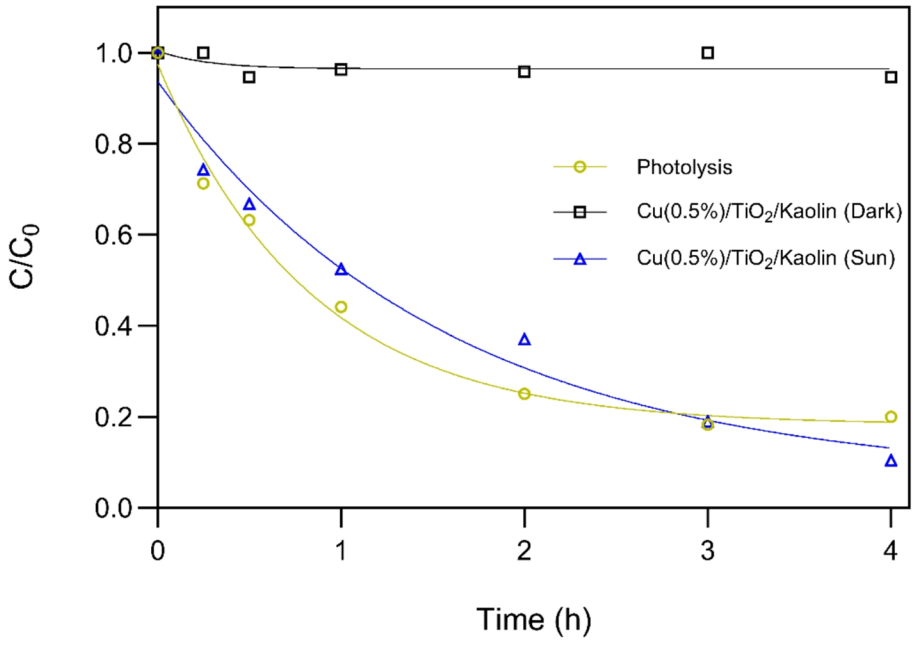


Fig. 4 Degradation of diclofenac, at an initial concentration of 25 mg/L, under direct sunlight (photolysis) and with Cu (0.5%)/TiO_2/Kaolin under dark and sunlight

3.2 Photocatalytic activity of Cu (0.5%)/TiO_2/Kaolin thin-films

Direct photolysis can induce structural modifications or lead to the decomposition of pollutant compounds through the direct or indirect action of absorbed light [44–46]. In this work, photolysis resulted in a significant removal of DCF, reaching 80% in DW, under sunlight after 4 h (Fig. 4). Similar findings were reported by Li et al. [47]., who observed 67% DCF removal in DW by photolysis under simulated sunlight (with a solar intensity of 100 mW/cm^2), in just 2 h of irradiation, with DCF concentrations as high as 100 mg/L. It has also been reported that, under sunlight, the initial molecule of DCF undergoes rapid degradation into other transformation products through mechanisms such as substitution, dechlorination, dihydroxylation, homodimerization and heterodimerization [47]. DCF shows high susceptibility to direct photolysis due to its molecular structure, which readily absorbs UV light within the 254–280 nm range, a spectral region present in natural sunlight [48]. This property facilitates photochemical reactions, accounting for the rapid structural modifications and decomposition of DCF observed under direct solar irradiation in the absence of a photocatalyst.

Despite this notable photolytic activity, the incorporation of Cu (0.5%)/TiO_2/Kaolin thin films significantly enhanced both the degradation rate and final removal efficiency. Under sunlight irradiation, DCF removal considerably increased, reaching 89.48% within only 4 h of sunlight exposition, a value nearly 10% higher than photolysis alone. Moreover, the observed degradation rate also improved from 0.402 h^{-1} (photolysis) to 0.563 h^{-1} in the presence of Cu(0.5%)/TiO_2/Kaolin, 0.563 h^{-1}. In contrast, under dark conditions, the catalyst showed negligible activity (only 6% removal), confirming the photocatalytic nature of the process. These results indicate that the use of Cu(0.5%)/TiO_2/Kaolin enables the reaction to progress further, reaching higher levels of degradation compared to photolysis alone.

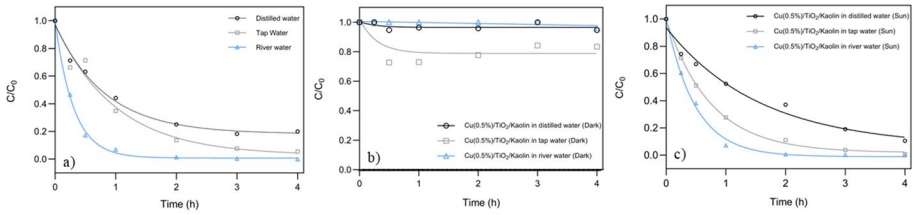


Fig. 5 Influence of different water matrices in the removal of diclofenac, at an initial concentration of 25 mg/L: (**a**) Photolysis; (**b**) Cu(0.5%)/TiO_2/Kaolin under dark conditions; (**c**) Cu(0.5%)/TiO_2/Kaolin under solar irradiation

Table 3 Percentage of DCF removal after 2 h and 4 h of process without catalyst (photolysis) and in the presence of Cu(0.5%)/TiO_2/Kaolin catalyst under dark and under solar irradiation, for different water matrices and DCF concentrations

Conditions	Water matrix	DCF Concentration (mg/L)	Removal at 2 h irradiation (%)	Removal at 4 h irradiation (%)	Rate constant (h^{-1})
Photolysis	DW	25	74.92	80.00	0.402
	TW		86.32	94.58	0.729
	RW		98.69	100	1.875
Cu(0.5%)/TiO_2/Kaolin Dark conditions	DW		4.20	5.36	0.014
	TW		22.32	16.59	0.045
	RW		0	3.96	0.010
Cu(0.5%)/TiO_2/Kaolin Solar irradiation	DW	100	89.67	98.70	1.086
		25	62.93	89.48	0.563
		1	98.43	100	2.076
		0.5	100	100	3.071
	TW	100	35.38	55.74	0.204
		25	88.87	99.37	1.266
		1	97.85	100	1.920
		0.5	67.48	100	0.524
	RW	100	34.40	63.93	0.255
		25	99.40	100	2.301
		1	98.68	100	2.293
		0.5	100	100	2.667

The improvement in the presence of the catalyst, may be attributed to distinct mechanisms involved in heterogeneous photocatalysis, wherein the activation of the semiconductor (TiO_2) by sunlight generates RO), such as •OH and O_2•$^-$, which non-selectively attack organic pollutants and promote more extensive degradation. This is fundamentally different from photolysis, which relies on direct light absorption by the pollutant itself and leads mainly to partial transformation. Furthermore, the use of supported photocatalysts, such as Cu-TiO_2 immobilized on kaolin, offers added value for long-term operation, as it facilitates catalyst recovery, minimizes nanoparticle leaching, and promotes sustained activity over multiple cycles. This makes the system not only effective in accelerating pollutant breakdown but also more viable for practical applications aiming at complete mineralization and reuse of treated water.

3.2.1 Influence of different water matrices in the photocatalytic activity of Cu (0.5%)/TiO_2/Kaolin thin-film

The complexity of water matrices can influence both photolysis and photocatalysis [49]. In this study, the catalytic performance was evaluated in three different types

of water, DW, TW and RW, all of which exhibiting neutral pH values. The first-order kinetic curves for DCF degradation in the different water matrices are shown in Fig. 5. Removal percentages and corresponding rate constants for all tested concentrations, are present in Table 3. Photolysis exhibited distinct behaviors across matrices, with particularly rapid degradation observed in river water (RW) (Fig. 5a). In RW, the photolysis process was faster, with almost complete removal occurring within 2 h, while in other matrices, DW and TW, photolysis after 2 h reached 80% and 86.32%, respectively. The degradation rate in RW was approximately 2.5 times higher than in TW and around 5 times higher than in DW. Near-complete degradation in TW was achieved within 4 h (Table 3). These different results may be related to the varying compositions of the water matrices, which highly influence the degradation efficiency of DCF. One possible explanation for the increased photolysis in RW compared to the other water matrices is the presence of nitrate ions, which can enhance the production of hydroxyl radicals, as discussed in the review by Ahmad et al. [50]. To investigate this, nitrate levels were measured in the three used water matrices. As expected, RW contained considerably higher levels of nitrates than TW, with concentrations of 2.49 mg/L in RW and 0.24 mg/L in TW, respectively, while no nitrates were detected in DW. A study by Kanakaraju et al. [51], also reported high DCF photolysis (at an initial concentration of 30 mg/L) under sunlight in RW and TW matrices, 82% and 84%, respectively, in approximately 6 h under direct sunlight, achieving higher removal extents than using TiO_2 for the photocatalytic process. However, photolysis is not a consistent technology, as many factors can interfere with its efficiency, such as sunlight intensity and the presence of organic matter in the different water matrices.

Regarding the assays with Cu(0.5%)/TiO_2/Kaolin performed under dark conditions, similar results were achieved for DW and RW, with adsorption extents of 5.36% and 3.96%, respectively. However, in TW adsorption was higher, 16.59%, although still relatively low (Table 3). In the assays under solar irradiation, the presence of Cu(0.5%)/TiO_2/Kaolin enhanced the degradation rate of DCF, with RW demonstrating the highest degradation, followed by TW and DW, respectively (Fig. 5c). Complete removal was achieved with RW after half the irradiation time (Table 3). Notable, the degradation in TW was also higher than the obtained by photolysis (Fig. 5a and c), with almost complete removal after 4 h, and at an almost doubled rate (0.729 h^{-1} for photolysis and 1.266 h^{-1} with the catalyst). These results indicate that the application of the Cu(0.5%)/TiO_2/Kaolin catalyst enhances the removal of DCF under sunlight, particularly in natural waters such as TW and RW.

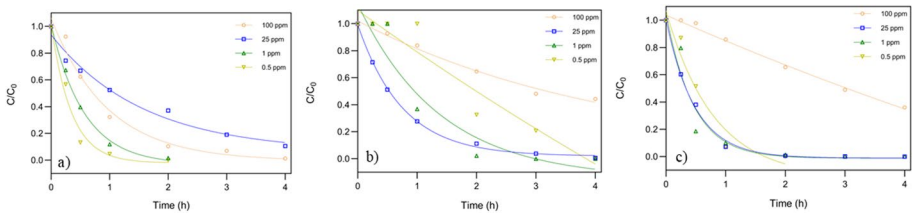


Fig. 6 DCF removal in different water matrices and at varying initial DCF concentrations: (**a**) Distilled water, (**b**) Tap Water; (**c**) River Water

3.2.2 Effect of DCF concentration in Cu (0.5%)/TiO_2/Kaolin thin-film photocatalytic activity

Different concentrations of pollutants may affect the photocatalytic performance of a given photocatalyst. It is well established that as the concentration of DCF increases, a corresponding decrease in degradation efficiency is commonly observed [52, 53]. In this study, four different DCF concentrations were tested, two within the typical environmental range (0.5 mg/L and 1 mg/L) and two at significantly higher levels (25 mg/L and 100 mg/L) [6]. Interestingly, in DW, Cu(0.5%)/TiO_2/Kaolin exhibited a faster and higher final removal of DCF at a concentration of 100 mg/L compared to 25 mg/L (Fig. 6a). After 4 h of irradiation, nearly complete removal was achieved at 100 mg/L (rate of 1.086 h^{-1}) compared to 89.48% removal at 25 mg/L (rate of 0.563 h^{-1}) (Table 2). This enhanced degradation at higher concentrations is likely attributed to availability of pollutant molecules, where a greater number of initial DCF molecules are available to interact with the photocatalyst's surface, leading to increased photon absorption and subsequently accelerating the degradation process [52]. As the concentration reaches values close to those detected in the environment, the DCF degradation rate increases significantly, as expected. At 1 and 0.5 mg/L, nearly complete removal (98.43%) was achieved in just 2 h, with a degradation rate of 2.076 h^{-1}. At half this concentration, DCF is no longer detected after 2 h of solar irradiation, exhibiting a superior degradation rate of 3.071 h^{-1}. In TW (Fig. 6b) and RW (Fig. 6c), increasing concentrations of DCF also influence its removal percentage and rate constant, although differently than the tendency on DW. After 4 h of irradiation, total removal was achieved for the lowest concentrations (0.5, 1 and 25 mg/L), while 44.26% of DCF remained for 100 mg/L (Table 2). The degradation rate was notably higher for 1 mg/L DCF, reaching 1.920 h^{-1}, approximately 9-fold faster than with 100 mg/L, 4-fold faster than with 0.5 mg/L and 1.5-fold faster than for 25 mg/L (Table 2). Identical results were observed in the assays with RW (Fig. 6c), showing a clear concentration-dependent activity. The lowest concentrations exhibited faster removal rates, with 100% degradation achieved for 0.5 mg/L after 2 hs of solar irradiation, corresponding to a degradation rate of 2.667 h^{-1}, and 98,68% for 1 mg/L at a rate of 2.293 h^{-1}. Interestingly, even with a significant increase of DCF to 25 mg/L, the degradation rate remained in the similar range, 2.644 h^{-1}, indicating that variations in DCF concentration between 0.5 and 25 mg/L produce comparable results. As seen previously with TW, the higher concentration tested, 100 mg/L, significantly hindered the efficiency of Cu (0.5%)/TiO_2/Kaolin, leading only to 14.19% DCF removal after the first h of irradiation. Nevertheless, considerable higher DCF removal was obtained in RW (64.93%, rate of 0.255 h^{-1}) than in TW (55.74%, rate of 0.204 h^{-1}).

The effects differ significantly in TW and RW compared to DW, primarily due to the presence of inorganic ions and natural organic matter, which can interfere with the photocatalytic process. The ions commonly present in TW, such as chloride (Cl^-) and sulphates (SO_4^{2-}), absent in DW, may also contribute to the observed differences in behavior between the two different water matrices [50]. These constituents may lead to surface fouling or blockage of active sites on the photocatalyst, as well as light scattering, both of which reduce photocatalytic efficiency. At high DCF concentrations (e.g., 100 mg/L), these interferences become more pronounced, as the number of pollutant molecules competing for fewer available active sites increases. Additionally, the catalyst's active areas may be insufficient to effectively process such high pollutant loads under these conditions, explaining the observed lower removal efficiencies in TW and RW.

Table 4 Results of HPLC-MS obtained after 2 h of solar irradiation of a diclofenac (DCF) solution in deionized water, in the presence of Cu (0.5%)/TiO_2/Kaolin thin film

Retention Time (min)*	Experimental m/z	Nominal mass (g/mol)	Chemical Formula
18.51	296.12	296	$C_{14}H_{11}Cl_2NO_2$
16.14	312.08	312	$C_{14}H_{11}Cl_2NO_3$
17.49	260.04	260	$C_{14}H_{11}ClNO_2$
14.78	242.06	242	$C_{14}H_{10}ClNO$
17.48	214.10	214	$C_{13}H_{10}ClN$
15.82	310.17	310	$C_{14}H_{10}Cl_2NO_3$
15.25	278.13	278	$C_{14}H_{10}Cl_2NO$
16.14	180.67	180	$C_{13}H_{10}N$
16.14	332.42	332	$C_{14}H_{11}Cl_3NO_2$
14.78	304.42	304	$C_{13}H_{11}Cl_3NO$
12.78	274.33	274	$C_{11}H_9Cl_3NO$
15.22	495.21	495	$C_{26}H_{20}Cl_3N_2O_2$
15.82	481.13	481	$C_{25}H_{19}Cl_3N_2O_2$

*, The products with the same retention time are confirmed by extracted chromatogram in SIM mode

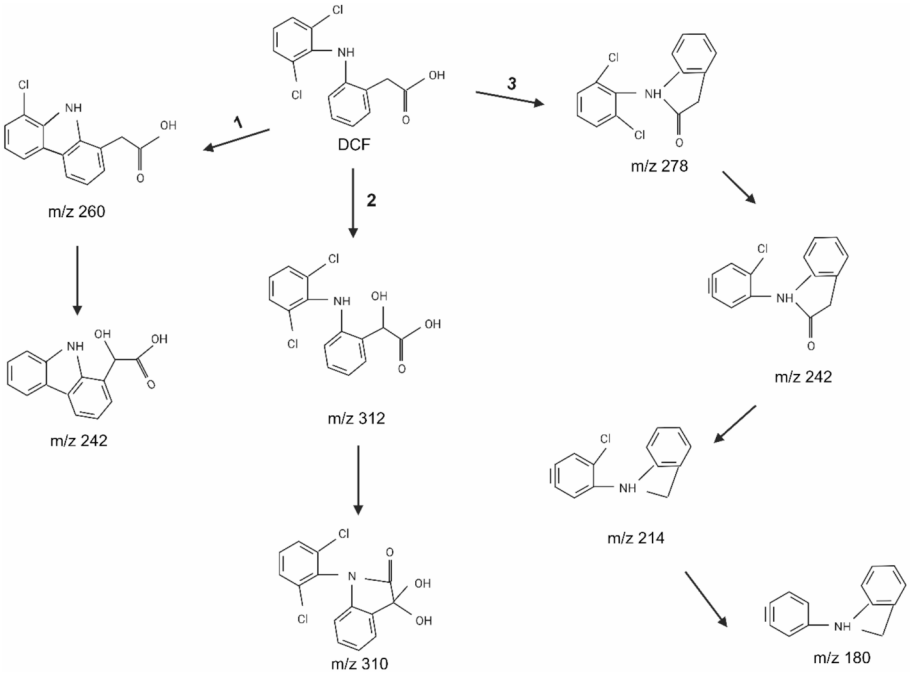


Fig. 7 Proposed degradation mechanisms and pathways of DCF under photocatalysis with Cu(0.5%)/TiO_2/Kaolin under solar irradiation

The results with varying DCF initial concentration, also highlight how different matrices impact the photocatalytic performance of Cu(0.5%)/TiO_2/Kaolin for DCF removal. Notably, the Cu(0.5%)/TiO_2/Kaolin catalyst performed better at higher concentrations of DCF, i.e. 100 mg/L, in more purified water, likely due to the absence of competing substances such as salts and natural organic matter. In TW and RW, these constituents may suppress the interaction between the pollutant and the catalyst by occupying active sites or scattering light, thus hindering photocatalytic efficiency. In contrast, in more purified water, the interaction between Cu(0.5%)/TiO_2/Kaolin and photons is likely enhanced, as there is less light scattering and reduced competition for light absorption. At lower DCF

concentrations, the catalyst maintained high removal rates across all matrices, indicating its suitability for practical applications even under environmentally relevant conditions.

3.3 Transformations products and degradation mechanisms of DCF

The transformation products during the photocatalytic degradation of DCF, under solar irradiation using Cu(0.5%)/TiO_2/Kaolin in DW, were analyzed by HPLC-MS (Table 4). A total of 13 structures were identified through their *m/z* values. Drawing on these identified compounds and established degradation mechanisms reported in the literature, plausible reaction pathways for the photocatalytic degradation of DCF were proposed, as illustrated in Fig. 7.

Based on the obtained *m/z* values, DCF may undergo degradation through three distinct pathways: (1) loss of chlorine followed by cyclization [47], resulting in the compound with *m/z* = 260.04, which may be addressed as 2-(8-chloro-9 H-carbazol-1-yl) acetic acid; (2) hydroxylation due to the attack of hydroxyl radicals ($OH^{\bullet}$), as evidenced by the ion detected at *m/z* = 312.12 [54]; (3) water loss from DCF, giving the ion at *m/z* = 278 [55]. The pathway 1 continues with the dechlorination-hydroxylation of *m/z* = 260.04, forming the transformation product identified at *m/z* = 242.06, which may be assigned to 8-chlorocarbazole-1-acetic acid [56]. Hydroxylation can also proceed via pathway 2, followed by the detection of *m/z* 310, which may be assigned to the compound 1-(2,6-dichlorophenyl)–3,3-dihydroxyindolin-2-one. According to [57], this transformation product results from a double hydroxylation of DCF, which was not detected in the present study, with further loss of a water molecule (H_2O). Regarding pathway 3, the compound at *m/z* = 278 (Fig. 7), can be further degraded, as supported by the detected transformation products with *m/z* = 242 and *m/z* = 214. The formation of *m/z* = 242 likely results from the loss of a chlorine atom from the compound at m/z 278. The subsequent loss of a single chlorine atom along with a CO group [55] leads to the formation of the ion at m/z 214. Further loss of an additional chlorine atom then results in the formation of the ion at m/z 180.

The ion at *m/z* = 332 may be attributed to a chlorinated DCF, likely resulting from the presence of chlorine in the water matrix or from supporting material. The identification of another ion, at *m/z* = 304, further supports this additional pathway, suggesting the loss of CO from the chlorinated species. Further, the loss of a CH_2O (Formaldehyde) may lead to the formation of the transformation product identified at *m/z* = 274.35.

Some ions with higher *m/z* ratios were also identified (Table 4), which may possibly result from the dimerization of DCF. Formation of a dimerization product of DCF at *m/z* = 589, also observed during photocatalysis, has been reported by O. S. Keen (2013), who attributed it to the formation of dimer-derived structures [58]. In the present work, ions at *m/z* = 495 and *m/z* = 481 were detected. It is suggested that the transformation product at *m/z* = 495 forms from successive losses of CO_2, CH_3 and Cl from a dimer of DCF, while the further loss of a CH_2 group may explain the formation of detected ion at *m/z* = 481. Further into the correspondent pathways, low molecular carboxylic acid may also be formed.

3.4 Toxicity assays

To comprehensively evaluate the performance of Cu (0.5%)/TiO_2/Kaolin, it is crucial to assess the toxicity of the treated effluent. This evaluation provides valuable insights into

Table 5 Percentage of luminescence Inhibition (INH%) of the performed assays using Cu (0.5%)/TiO_2/Kaolin in different matrices and conditions

Sample description	Water matrix	Degradation Treatment	DCF (mg/L)	INH%	Toxicity interpretation
Positive control ($K_2Cr_2O_7$)	DW	n.a.	0	88.3 ± 0.4	Very Toxic
Tap Water	TW			0 ± 0.3	Negligible
River Water	RW			0 ± 0.7	Negligible
Without catalyst	DW	Photolysis, 0 h	25	98.7 ± 0.2	Very Toxic
		Photolysis, 4 h		46.8 ± 0.3	Toxic
Cu(0.5%)/TiO_2/Kaolin		Dark, 4 h		99 ± 0.2	Very Toxic
		Solar irradiation, 4 h		47.5 ± 0.8	Toxic
		Solar irradiation, 0 h	100	99.7 ± 0.1	Very Toxic
		Solar irradiation, 4 h		78.9 ± 0.3	Very Toxic
		Solar irradiation, 0 h	1	41.1 ± 0.9	Toxic
		Solar irradiation, 4 h		39.7 ± 0.3	Toxic
		Solar irradiation, 0 h	0.5	44.6 ± 0.5	Toxic
		Solar irradiation, 4 h		39.2 ± 1.0	Toxic
	TW	Solar irradiation, 0 h	100	99.6 ± 0.0	Very Toxic
		Solar irradiation, 4 h		80.7 ± 0.5	Very Toxic
	RW	Solar irradiation, 0 h		99.±0.5	Very Toxic
		Solar irradiation, 4 h		44.6 ± 0.5	Toxic
	DW	UV, 4 h		99.2 ± 0.1	Very Toxic
	TW			98.9 ± 0.0	Very Toxic
	RW			99.5 ± 0.0	Very Toxic

the toxicity dynamics throughout the treatment process, allowing for the determination of whether the degradation of the parent compound results in effective detoxification or if transformation products persist in the final effluent and cause toxicity. Additionally, it allows for the assessment of the catalyst's safety, ensuring that its use does not introduce or contribute to adverse toxic effects in the treated water. The degree of luminescence inhibition observed in the assays is presented in Table 5.

To assess the influence of different water matrices on toxicity, TW and RW were also evaluated for their effects on *Vibrio fischeri*. Both matrices exhibited negligible toxicity in the absence of DCF. However, the presence of DCF (samples 0 h) significantly increased toxicity, reaching nearly 100% inhibition, regardless of the water matrix, at a DCF concentration of 100 mg/L. When the concentration of DCF was reduced to 25 mg/L in DW, which also exhibited negligible baseline toxicity, inhibition values remained high, with toxicity reaching 98.7–99,7%. These findings classify DCF as "very toxic" to *V. fischeri* [32, 59]. Previous studies have also highlighted the acute toxicity of DCF to *V. fischeri*. For instance, Zhang et al. [7]. reported an EC_{50} (the concentration that causes 50% inhibition) of 11.45 mg/L, and Kovacic et al. [60]., observed a comparable Ec_{50} of 14.47 mg/L. Additionally, Fischer et al. [61]., reported an Ec_{50} value of 19.7 mg/L DCF. These reference values align with the results observed in the present study, which demonstrate that higher DCF concentrations (25 mg/L and 100 mg/L) significantly increase toxicity. As the DCF concentration decreases, the associated toxicity also diminishes. For instance, at concentrations of 1 and 0.5 mg/L in DW, the toxicity dropped to 41.1% and 44.6%, respectively, both of which still classify as 'toxic', but represent a substantial reduction in toxicity. This demonstrates the concentration-dependent nature of DCF toxicity towards *V. fischeri*.

DCF is known to exhibit toxicity not only in its original form but also through its metabolites generated during various treatment processes. Photolysis, which involves sunlight exposure without the use of a catalyst, effectively promoted the degradation of DCF. Following 4 h of sunlight exposure, a solution containing 25 mg/L of DCF in DW exhibited a significant reduction in toxicity, with inhibition levels decreasing from 98.7 to 46.8%. In the presence of Cu(0.5%)/TiO_2/Kaolin under dark conditions, no significant changes in toxicity were observed after 4 h of contact at the same concentration and water matrix. However, when exposed to solar irradiation, a reduction in toxicity occurred, reaching levels comparable to photolysis, albeit with previously noted higher removal efficiency and removal rates. As the DCF concentration increased from 25 mg/L to 100 mg/L, the efficiency of Cu(0.5%)/TiO_2/Kaolin on detoxification decreased, and while toxicity remained within the "very toxic" range, it was reduced from 99.7 to 78.9%. At realistic DCF concentrations of 1 mg/L and 0.5 mg/L, toxicity decreased from 41.1 to 39.7% and from 44.6 to 39.2%, respectively, reflecting a reduction of approximately 3.4 and 12% for 1 and 0.5 mg/L DCF, respectively. A similar trend is observed across different water matrices with Cu(0.5%)/TiO_2/Kaolin, where toxicity decreases following treatment. In TW, at a DCF concentration of 100 mg/L and a removal efficiency of 55.74% after 4 h of sunlight exposure, toxicity was reduced from 99.6% (initial) to 80.7%. In RW, a more pronounced decrease in toxicity was noted, dropping from 99 to 44.6% with a removal efficiency of 63.93%, demonstrating the superior effectiveness of Cu(0.5%)/TiO_2/Kaolin in real water systems, particularly in RW.

Several studies have reported that the transformation products of DCF can exhibit higher toxicity than the parent compound [61, 62]. This increased toxicity is often associated with the formation of hydroxylated, carboxylated, or decarboxylated species during degradation [63]. The toxicity profile varies depending on the degradation stage, as different transformation products are generated throughout the process. In the present work, a decrease in toxicity was observed after 4 h of solar irradiation at a concentration of 100 mg/L. However, under UV light, despite the rapid degradation of the parent DCF compound, toxicity remained close to 100%. The products formed under solar irradiation, such as hydroxylated species (e.g., 311DCF, 267DCF) and dechlorinated species, likely contribute to the residual toxicity. The release of free chlorine, as highlighted in the review by Nosek and Zhao [63], may also contribute to that residual toxicity. In addition to the aforementioned factors, other mechanisms likely contribute to the observed increase in toxicity, particularly in the UV assays [63]. Notably, in experiments using 100 mg/L DCF under UV irradiation, the initially transparent water developed brownish tones and turbidity, a phenomenon not observed in assays conducted under dark conditions, where transparency was maintained. This turbidity is attributed to the formation of products such as carbazole dimers and other colored dimers, as noted by [64]. The formation of these compounds is supported by the detection of transformation products under UV irradiation, including various dimerization products such as 440DCF, 460DCF, and 454DCF, which contribute to the altered optical properties and may enhance toxicity. Another plausible explanation for the increased turbidity is the oxidation of DCF's aromatic rings, which can signal a more advanced stage of degradation under UV light, and contribute to the observed changes in water clarity, as suggested by [65]. These results demonstrate the variation in toxicity across different degradation stages, emphasizing the importance of assessing toxicity alongside degradation efficiency. Prolonged solar exposure in the presence of Cu (0.5%)/TiO_2/Kaolin could further enhance the degradation

process, driving DCF to more advanced degradation stages and ultimately achieving complete mineralization and detoxification. Beside extending the photocatalytic treatment duration, additional strategies could be explored to mitigate the residual toxicity associated with degradation by-products. These include applying sequential treatments to promote further mineralization, combining photocatalysis with biological post-treatment to enhance detoxification, implementing adsorptive post-treatments such as activated carbon, and optimizing the photocatalyst formulation to favor complete breakdown of toxic intermediates.

4 Conclusions

In this study, Cu(0.5%)/TiO_2/Kaolin thin films were successfully synthesized and evaluated for their photocatalytic efficiency in degrading DCF. The prepared films demonstrated high efficacy under solar irradiation, achieving faster and more significant DCF removal compared to photolysis alone. The catalyst showed robust performance across different water matrices, including deionized water, tap water, and river water, indicating its versatility for real-world applications. Various transformation products were identified during the degradation process, suggesting multiple degradation pathways, such as hydroxylation, decarboxylation, and dechlorination. Under UV irradiation, more advanced degradation stages were achieved, pointing to the possibility of complete mineralization of DCF with extended solar exposure. Additionally, the Cu(0.5%)/TiO_2/Kaolin catalyst, supported on thin films, is easily retrievable from reactors and can be regenerated for reuse, making it highly suitable for industrial applications. Toxicity assays with *Vibrio fischeri* revealed that while DCF significantly increases toxicity in water systems, the use of Cu(0.5%)/TiO_2/Kaolin under solar irradiation effectively reduces this toxicity, even at higher DCF concentrations, although final solutions remained "toxic." The reduction in toxicity was more pronounced in river water (RW), highlighting the catalyst's potential for treating polluted natural water sources. However, under UV light, despite rapid DCF degradation, toxicity remained nearly 100%. Further investigations are needed to fully understand the degradation mechanisms and ensure complete detoxification of treated effluents. Moreover, although the catalyst demonstrated strong stability and performance, the evaluation of potential metal leaching from the Cu-TiO_2/Kaolin films was not included in the scope of the present study. Considering the relevance of this aspect to environmental safety and long-term catalyst stability, future work should incorporate systematic leaching analyses under various operational conditions. Overall, Cu(0.5%)/TiO_2/Kaolin thin films hold significant promise for industrial-scale applications in water treatment, providing an effective and adaptable solution for the removal of micropollutants such as DCF from diverse water matrices.

Acknowledgements

This research was carried out in the framework of grant PID2021-127898OB-I00 (WAntRed), funded by MICIU/AEI and 'ERDF: A way of making Europe'. Financial support was also provided by the regional government of the Xunta de Galicia through project GRC/ED431C 2023/33. SST is grateful to the Erasmus+ program for a mobility grant. This study was supported by the Portuguese Foundation for Science and Technology (FCT) under the scope of the strategic funding of CF-UM-UP (UIDB/04650/2020, UIDP/04650/2020) and CEB (UIDB/04469/2020, UIDP/04469/2020), and by LABBELS–Associate Laboratory in Biotechnology, Bioengineering and Microelectromechanical Systems, LA/P/0029/2020. R.J.C. Fernandes acknowledges FCT for the PhD grant 2021.08418.BD.

Author contributions

Conceptualization– R.J.C. Fernandes, S.S. Tlemcani, and L. Pereira; Funding acquisition– M. Canle; Investigation– R.J.C. Fernandes, S.S. Tlemcani and A.R. Pereira; Methodology– R.J.C. Fernandes, S.S. Tlemcani, A.R. Pereira and L. Pereira; Project administration– L. Pereira and M. Canle; Resources - L. Pereira, M. Canle and P. Parpot; Supervision - L. Pereira, M. Canle and P. Parpot; Validation - L. Pereira, M. Canle and P. Parpot; Writing, original draft - R.J.C. Fernandes; Writing, review and editing - L. Pereira, M. Canle and P. Parpot.

Data availability
All data generated or analysed during this study are included in this published article [and its supplementary information files].

Declarations

Ethics and consent to participate
Not applicable.

Consent to publication
Not applicable.

Competing interests
The authors declare no competing interests.

Clinical trial number
Not applicable.

Received: 15 April 2025 / Accepted: 18 July 2025
Published online: 22 August 2025

References

1. de Souza H, Costa RdosS, Quadra GR, Fernandez MA. Pharmaceutical pollution and sustainable development goals: Going the right way? *Sustain. Chem. Pharm.*, vol. 21, no. April, 2021, https://doi.org/10.1016/j.scp.2021.100428
2. Mosharaf MK, Gomes RL, Cook S, Alam MS, Rasmusssen A. Wastewater reuse and pharmaceutical pollution in agriculture: uptake, transport, accumulation and metabolism of pharmaceutical pollutants within plants. Chemosphere. 2024;364(May). https://doi.org/10.1016/j.chemosphere.2024.143055.
3. Silva AR, Mesquita DP, Salomé Duarte M, Lado Ribeiro AR, Pereira MFR, Madalena Alves M, Monteiro S, Santos R, Cunha MV, Jorge S, Vieira J, Vilaça J, Lopes LC, Carvalho M, Brito C, Martins A. Exploring the correlations between Epi indicators of COVID-19 and the concentration of pharmaceutical compounds in wastewater treatment plants in Northern Portugal. J Hazard Mater Adv. 2023;10:100315. https://doi.org/10.1016/j.hazadv.2023.100315.
4. Landsdorp D, Vree TB, Janssen TJ, Guelen PJ. Pharmacokinetics of rectal diclofenac and its hydroxy metabolites in man, *Int. J. Clin. Pharmacol. Ther. Toxicol.*, vol. 28, no. 7, pp. 298–302, Jul. 1990, [Online]. Available: http://europepmc.org/abstract/MED/2387653
5. Andreozzi R, Marotta R, Paxéus N. Pharmaceuticals in STP effluents and their solar photodegradation in aquatic environment. Chemosphere. 2003;50(10):1319–30. https://doi.org/10.1016/S0045-6535(02)00769-5.
6. Rizzo L, Meric S, Kassinos D, Guida M, Russo F, Belgiorno V. Degradation of diclofenac by TiO2 photocatalysis: UV absorbance kinetics and process evaluation through a set of toxicity bioassays. Water Res. 2009;43(4):979–88. https://doi.org/10.1016/j.watres.2008.11.040.
7. Zhang Y, Geißen SU, Gal C. Carbamazepine and diclofenac: Removal in wastewater treatment plants and occurrence in water bodies, *Chemosphere*, vol. 73, no. 8, pp. 1151–1161, 2008, https://doi.org/10.1016/j.chemosphere.2008.07.086
8. Taggart MA, Senacha KR, Green RE, Jhala YV, Raghavan B, Rahmani AR, Cuthbert R, Pain DJ. A.A A. Meharg., Diclofenac residues in carcasses of domestic ungulates available to vultures in India, *Environ. Int.*, vol. 33, no. 6, pp. 759–765, 2007, https://doi.org/10.1016/j.envint.2007.02.010
9. Shamsudin MS, Azha SF, Ismail S. A review of diclofenac occurrences, toxicology, and potential adsorption of clay-based materials with surfactant modifier. J Environ Chem Eng. 2022;10(3):107541. https://doi.org/10.1016/j.jece.2022.107541.
10. Nassiri Koopaei N, Abdollahi M. Health risks associated with the pharmaceuticals in wastewater. DARU J Pharm Sci. 2017;25(1):1–7. https://doi.org/10.1186/s40199-017-0176-y.
11. Malato S, Blanco J, Vidal A, Richter C. Photocatalysis with solar energy at a pilot-plant scale: an overview. Appl Catal B Environ. 2002;37(1):1–15. https://doi.org/10.1016/S0926-3373(01)00315-0.
12. Li Puma G, Toepfer B, Gora A. Photocatalytic oxidation of multicomponent systems of herbicides: Scale-up of laboratory kinetics rate data to plant scale. Catal Today. 2007;124:3–4. https://doi.org/10.1016/j.cattod.2007.03.047.
13. Khan H, Rigamonti MG, Patience GS, Boffito DC. Spray dried TiO2/WO3 heterostructure for photocatalytic applications with residual activity in the dark, *Appl. Catal. B Environ.*, vol. 226, no. November 2017, pp. 311–323, 2018. https://doi.org/10.1016/j.apcatb.2017.12.049
14. Khan MI, Mujeeb M, Farooq U. Sol-gel deposition and electrical properties of laser irradiated Cu doped TiO2 multilayer thin films. Results Phys. 2017;7:2485–8. https://doi.org/10.1016/j.rinp.2017.07.038.
15. Bensouici F, et al. Optical, structural and photocatalysis properties of Cu-doped TiO 2 thin films. Appl Surf Sci. 2017;395:110–6. https://doi.org/10.1016/j.apsusc.2016.07.034.
16. Wang S, Meng KK, Zhao L, Jiang Q, Lian JS. Superhydrophilic Cu-doped TiO2 thin film for solar-driven photocatalysis. Ceram Int. 2014;40(4):5107–10. https://doi.org/10.1016/j.ceramint.2013.09.028.
17. Tlemcani SS, Santaballa JA. Treatment of aqueous amoxicillin solutions with sunlight using a pelletized macrocomposite photocatalyst. Materials. 2025;18:1394.
18. Asmare ZG, Aragaw BA, Atlabachew M, Wubieneh TA. Kaolin-Supported silver nanoparticles as an effective catalyst for the removal of methylene blue dye from aqueous solutions. ACS Omega. 2023;8(1):480–91. https://doi.org/10.1021/acsomega.2c05265.
19. Ayodele OB, Lim JK, Hameed BH. Degradation of phenol in photo-Fenton process by phosphoric acid modified Kaolin supported ferric-oxalate catalyst: optimization and kinetic modeling. Chem Eng J. 2012;197:181–92. https://doi.org/10.1016/j.cej.2012.04.053.

20. Ayodele OB, Abdullah AZ. Exploring kaolinite as dry methane reforming catalyst support: Influences of chemical activation, organic ligand functionalization and calcination temperature, *Appl. Catal. A Gen.*, vol. 576, no. December 2018, pp. 20–31, 2019. https://doi.org/10.1016/j.apcata.2019.02.034
21. El-Aal MA, Said AEAA, Abdallah MH, Goda MN. Modified natural Kaolin clay as an active, selective, and stable catalyst for methanol dehydration to dimethyl ether. Sci Rep. 2022;12(1):1–13. https://doi.org/10.1038/s41598-022-13349-0.
22. Nan M, Vimonses V, Lei S, Jin B, Chow C, Saint C. Microporous and mesoporous materials synthesis and characterisation of novel Titania impregnated kaolinite nano-photocatalyst. Microporous Mesoporous Mater. 2009;117:1–2. https://doi.org/10.1016/j.micromeso.2008.06.039.
23. Nan M, Lei S, Jin B, Saint C, Chow CWK. Optimisation of an annular photoreactor process for degradation of congo red using a newly synthesized Titania impregnated kaolinite nano-photocatalyst. Sep Purif Technol. 2009;67:355–63. https://doi.org/10.1016/j.seppur.2009.04.001.
24. Ko˘ci K, Mat˘ejka V, Ková˘r P, Lacný Z, Obalová L. Comparison of the pure TiO_2 and kaolinite / TiO_2 composite as catalyst for CO_2 photocatalytic reduction. Catal Today. 2011;161:105–9. https://doi.org/10.1016/j.cattod.2010.08.026.
25. Kibanova D, Trejo M, Destaillats H, Cervini-Silva J. Synthesis of Hectorite-TiO_2 nanocomposites with photocatalytic activity for the degradation of model air pollutants. Lawrence Berkeley National Laboratory; 2008. pp. 1–19.
26. Zyoud AH, Zubi A, Zyoud SH, Muath H, Hilal S, Zyoud N, Qamhieh AR, Hajamohideen HS, Hilal. Kaolin-supported ZnO nanoparticle catalysts in self-sensitized Tetracycline photodegradation: Zero-point charge and pH effects. Appl Clay Sci. 2019;182:105294. https://doi.org/10.1016/j.clay.2019.105294.
27. Mohammed KS, Atlabachew M, Aragaw BA, Asmare ZG. Synthesis of Kaolin-Supported nickel oxide composites for the catalytic oxidative degradation of methylene blue dye. ACS Omega. 2024;9(4):4287–99. https://doi.org/10.1021/acsomega.3c05126.
28. Standard I, Standard T. Iso 11348-1, vol. 1998, 1998.
29. Standard Methods Committee of the American Public Health Association, American Water Works Association. ISO 114348-3 - Water quality-Determination of the inhibitory effect of water samples on Te light emission of Vibrio fischeri (Luminescent bacteria Test)- part 3: method using freeze-dried bacteria. Stand Methods Exam Water Wastewater. 2023;2007:1–21.
30. Ohtani B, Prieto-Mahaney OO, Li D, Abe R. What is Degussa (Evonic) P25? Crystalline composition analysis, reconstruction from isolated pure particles and photocatalytic activity test. J Photochem Photobiol Chem. 2010;216:2–3. https://doi.org/10.1016/j.jphotochem.2010.07.024.
31. Ji K, Kim Y, Oh S, Ahn B, Jo H, Choi K. Toxicity of perfluorooctane sulfonic acid and perfluorooctanoic acid on freshwater macroinvertebrates (*Daphnia magna* and *Moina macrocopa*) and fish (Oryzias latipes). Environ Toxicol Chem. 2008;27(10):2159–68. https://doi.org/10.1897/07-523.1.
32. Silva AR, Soares OSGP, Pereira MFR, Alves MM, Pereira L. Tailoring carbon nanotubes to enhance their efficiency as Electron shuttle on the biological removal of acid orange 10 under anaerobic conditions. Nanomaterials. 2020;10:2496.
33. Silva AR, et al. Detoxification of Ciprofloxacin in an anaerobic bioprocess supplemented with magnetic carbon nanotubes: contribution of adsorption and biodegradation mechanisms. Int J Mol Sci. 2021;22(6):1–22. https://doi.org/10.3390/ijms22062932.
34. Silva AR, Sousa C, Exner D, Schwaiger R, Alves MM, Petrovykh DY, Pereira L. pH-induced modulation of *Vibrio fischeri* population life cycle. Chemosensors. 2021;9(10):1–14. https://doi.org/10.3390/chemosensors9100283.
35. Fujishima A, Honda K. Electrochemical photolysis of water at a semiconductor electrode. Nature. 1972;238(5358):37–8. https://doi.org/10.1038/238037a0.
36. Yitagesu GB, Leku DT, Seyume AM, Workneh GA. Biosynthesis of TiO2/CuO and its application for the photocatalytic removal of the methylene blue dye. ACS Omega. 2024. https://doi.org/10.1021/acsomega.4c03472.
37. Houas A, Lachheb H, Ksibi M, Elaloui E, Guillard C, Herrmann JM. Photocatalytic degradation pathway of methylene blue in water. Appl Catal B Environ. 2001;31(2):145–57. https://doi.org/10.1016/S0926-3373(00)00276-9.
38. Karunakaran C, Abiramasundari G, Gomathisankar P, Manikandan G, Anandi V. Cu-doped TiO_2 nanoparticles for photocatalytic disinfection of bacteria under visible light. J Colloid Interface Sci. 2010;352(1):68–74. https://doi.org/10.1016/j.jcis.2010.08.012.
39. Niu X, Du Y, Liu Y, Qi H, An J, Yang X, Feng Q. Hydrothermal synthesis and formation mechanism of the anatase nanocrystals with co-exposed high-energy {001}, {010} and [111]-facets for enhanced photocatalytic performance. RSC Adv. 2017;7(40):24616–27. https://doi.org/10.1039/c7ra03707d.
40. Wahyuni ET, Roto R, Novarita D, Suwondo KP, Kuswandi B. Preparation of TiO2/AgNPs by photodeposition method using Ag(I) present in radiophotography wastewater and their antibacterial activity in visible light illumination. J Environ Chem Eng. 2019;7(4):103178. https://doi.org/10.1016/j.jece.2019.103178.
41. Pongwan P, Wetchakun K, Phanichphant S, Wetchakun N. Enhancement of visible-light photocatalytic activity of Cu-doped TiO_2 nanoparticles. Res Chem Intermed. 2016;42(4):2815–30. https://doi.org/10.1007/s11164-015-2179-y.
42. Ganesh I, Kumar PP, Annapoorna I, Sumliner JM, Ramakrishna M, Helbalkar NY, Padmanabham G, Sundararajan G. Preparation and characterization of Cu-doped TiO_2 materials for electrochemical, photoelectrochemical, and photocatalytic applications. Appl Surf Sci. 2014;293:229–47. https://doi.org/10.1016/j.apsusc.2013.12.140.
43. Jiménez-Bautista K, Gascó A, Ramos DR, Palomo E, Muelas-Ramos V, Canle M, Hermosilla D, Bahamonde A. Solar-assisted photodegradation of pesticides over pellet-shaped TiO_2-kaolin catalytic macrocomposites at semi-pilot-plant scale: Elucidation of photo-mechanisms and water matrix effect. J Clean Prod. October, 2023;426. https://doi.org/10.1016/j.jclepro.2023.139203.
44. Wang L, Xu H, Lu J, Chovelon JM, Ji Y. Aquatic photolysis of the pharmaceutical ambroxol: the role of 2,4-dibromoaniline chromophore and heavy atom effect of bromine. Water Res. 2022;226:119275. https://doi.org/10.1016/j.watres.2022.119275.
45. Kounaris Fuziki ME, Ribas LS, Tusset AM, Brackmann R, Dos Santos OAA, Lenzi GG. Pharmaceutical compounds photolysis: pH influence, *Heliyon*, vol. 9, no. 2, p. e13678, 2023, https://doi.org/10.1016/j.heliyon.2023.e13678
46. Belikov YA, Snytnikova OA, Sheven DG, Fedunov RG, Grivin VP, Pozdnyakov IP. Laser flash photolysis and quantum chemical studies of UV degradation of pharmaceutical drug chloramphenicol: Short-lived intermediates, quantum yields and mechanism of photolysis, *Chemosphere*, vol. 351, no. December 2023, p. 141211, 2024. https://doi.org/10.1016/j.chemosphere.2024.141211

47. Li LP, Jin YC, Fang L, Zhang C. Direct photolysis of diclofenac under simulated sunlight: transformation pathway and biological concerns. Chemosphere. 2022;307:135775. https://doi.org/10.1016/j.chemosphere.2022.135775. no. P1.
48. Chianese S, Iovino P, Leone V, Musmarra D, Prisciandaro M. Photodegradation of diclofenac sodium salt in water solution: effect of HA, NO3− and TiO2 on photolysis performance. Water Air Soil Pollut. 2017;228(8). https://doi.org/10.1007/s11270-017-3445-y.
49. Petala A, Mantzavinos D, Frontistis Z. Impact of water matrix on the photocatalytic removal of pharmaceuticals by visible light active materials. Curr Opin Green Sustain Chem. 2021;28:100445. https://doi.org/10.1016/j.cogsc.2021.100445.
50. Ahmad S, Almehmadi M, Janjuhah HT, Kontakiotis G, Abdulaziz O, Saeed K, Ahmad H, Allahyani M, Aljuaid A, Alsaiari AA, Muhammad J, Khan I. The effect of mineral ions present in tap water on photodegradation of organic pollutants: future perspectives. Water (Switzerland). 2023;15(1). https://doi.org/10.3390/w15010175.
51. Kanakaraju D, Motti CA, Glass BD, Oelgemöller M. Photolysis and TiO2-catalysed degradation of diclofenac in surface and drinking water using Circulating batch photoreactors. Environ Chem. 2014;11(1):51–62. https://doi.org/10.1071/EN13098.
52. Lara-Pérez C, Leyva E, Zermeño B, Osorio I, Montalvo C, Moctezuma E. Photocatalytic degradation of diclofenac sodium salt: adsorption and reaction kinetic studies. Environ Earth Sci. 2020;79(11):1–13. https://doi.org/10.1007/s12665-020-09017-z.
53. Giahi M, ZnO C-doped. Russ J Appl Chem. 2015;88(12):2044–9. https://doi.org/10.1134/S10704272150120228.
54. Aghababaei N, Abdouss M, Hosseini-Monfared H, Ghanbari F. Photocatalytic degradation of diclofenac using a novel double Z-scheme catalyst (O-g-C_3N_4/ZnO/TiO_2@halloysite nanotubes): degradation mechanism, identification of by-products and environmental implementation. J Water Process Eng. 2023;53:103702. https://doi.org/10.1016/j.jwpe.2023.103702.
55. Galmier MJ, Bouchon B, Madelmont JC, Mercier F, Pilotaz F, Lartigue C. Identification of degradation products of diclofenac by electrospray ion trap mass spectrometry. J Pharm Biomed Anal. 2005;38(4):790–6. https://doi.org/10.1016/j.jpba.2005.02.016.
56. Zhang L, Liu Y, Fu Y. Degradation kinetics and mechanism of diclofenac by uv/peracetic acid. RSC Adv. 2020;10:9907–16. https://doi.org/10.1039/d0ra00363h.
57. Jiménez-Salcedo M, Monge M, Tena MT. The photocatalytic degradation of sodium diclofenac in different water matrices using g-C3N4 nanosheets: A study of the intermediate by-products and mechanism. J Environ Chem Eng. 2021;9(5):0–8. https://doi.org/10.1016/j.jece.2021.105827.
58. Keen OS, Thurman EM, Ferrer I, Dotson AD, Linden KG. Dimer formation during UV photolysis of diclofenac. Chemosphere. 2013;93(9):1948–56. https://doi.org/10.1016/j.chemosphere.2013.06.079.
59. Mendonc E, Picado A, Paixão SM, Silva L, Cunha MA, Leitão S, Moura I, Cortez C, Brito F. Ecotoxicity tests in the environmental analysis of wastewater treatment plants: case study in Portugal. J Hazard Mater. 2009;163:665–70. https://doi.org/10.1016/j.jhazmat.2008.07.012.
60. Kovacic M, Perisic DJ, Biosic M, Kusic H, Babic S, Bozic AL. RESEARCH ARTICLE UV photolysis of diclofenac in water; kinetics, degradation pathway and environmental aspects. Environ Sci Pollut Res. 2016;14908–17. https://doi.org/10.1007/s11356-016-6580-x.
61. Fischer K, Sydow S, Griebel J, Naumov S, Elsner C, Thomas I, Latif AA, Schulze A. Enhanced removal and toxicity decline of diclofenac by combining UVA treatment and adsorption of photoproducts to polyvinylidene difluoride. Polymers, *12*, 2340, 2020.
62. Schmitt-jansen M, Bartels P, Adler N, Altenburger R. Phytotoxicity assessment of diclofenac and its phototransformation products, pp. 1389–96, 2007, https://doi.org/10.1007/s00216-006-0825-3
63. Nosek K, Zhao D. Transformation products of diclofenac: formation, occurrence, and toxicity implication in the aquatic environment. Water Res. 2024;266:122388. https://doi.org/10.1016/j.watres.2024.122388.
64. Topkaya E. Treatability of diclofenac and triclosan solutions by catalytic and photocatalytic oxidation processes. J Chem Technol Biotechnol No June. 2024. https://doi.org/10.1002/jctb.7791.
65. Villota N, Echevarria B, De Luis A et al. Kinetic modelling of aromaticity and water colour changes during diclofenac oxidation by UV/H_2O_2, PREPRINT (Version 1) available at Research Square, 09 April 2024. https://doi.org/10.21203/rs.3.rs-4017935/v1

Publisher's note

Springer Nature remains neutral with regard to jurisdictional claims in published maps and institutional affiliations.